Sustained Solar-Powered Electrocatalytic H2 Production by Seawater Splitting Using Two-Dimensional Vanadium Disulfide

ACS Sustainable Chemistry & Engineering

pubs.acs.org/journal/ascecg

Research Article

Sustained Solar-Powered Electrocatalytic H_2 Production by Seawater Splitting Using Two-Dimensional Vanadium Disulfide

Paulraj Gnanasekar, Mathan Kumar Eswaran, Gayathri Palanichamy, Tien Khee Ng, Udo Schwingenschlögl, Boon S. Ooi, and Jeganathan Kulandaivel*

Cite This: https://doi.org/10.1021/acssuschemeng.1c01909

Read Online

ACCESS | Metrics & More | Article Recommendations | Supporting Information

ABSTRACT: Robust and stable electrodes made from earth-abundant materials have gained widespread interest in large-scale electrocatalytic water splitting toward hydrogen energy technologies. In this study, the vanadium disulfide (VS_2)/amorphous carbon (AC) heterostructure was employed as an electrode for direct seawater splitting. Two-dimensional VS_2 nanoparticles were deposited on AC with a high degree of uniformity via a well-optimized one-step chemical vapor deposition approach. The VS_2/AC heterostructure electrode was found to possess rich active sulfur sites, near-zero Gibbs free energy, a large surface area, and exceptional charge transfer toward the electrolyte, resulting in enhanced hydrogen evolution reaction (HER) performance with a low onset potential and low overpotential of 11 and 61 mV (vs reversible hydrogen electrode (RHE)), respectively. The electrode also sustained robust stability throughout the 50 h of chronoamperometry studies under acidic electrolyte conditions. Interestingly, the VS_2/AC electrocatalyst accomplished an exceptional HER performance under natural seawater conditions in the absence of an external electrolyte with an onset potential of 56 mV vs RHE and attained η_{200} at an overpotential of 0.53 V vs RHE. In spite of this, the heterostructure exhibited superior stability over 21 days at a high current density of 250 mA/cm^2 under both indoor and solar-powered outdoor conditions. Overall, this VS_2/AC heterostructure may open a new pathway toward direct seawater splitting for long-term, stable, large-scale hydrogen generation.

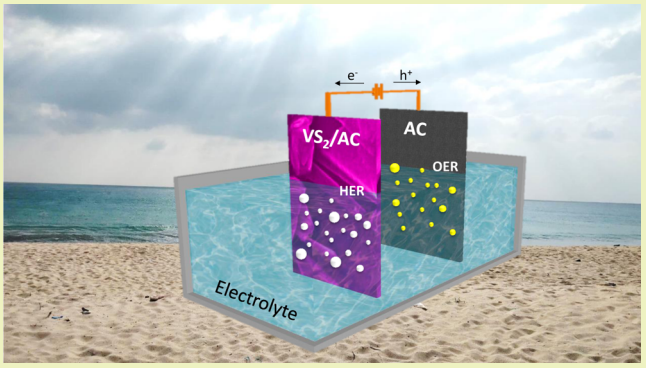

KEYWORDS: *seawater splitting, 2D materials, transition metal dichalcogenides, solar-powered, hydrogen production, density function theory, two-electrode water splitting*

INTRODUCTION

The goals of sustainable and alternative energy technology development efforts are to provide carbon-neutral fuels and solve expanding energy crises.[1,2] Currently, more than 80% of global energy requirements are satisfied using nonrenewable energy sources. Their sustained consumption harms society via environmental deterioration. Thus, there is a demand for alternative renewable energy sources.[3] Hydrogen is a future renewable energy candidate because of its high energy density (142 MJ/kg), abundance, and renewable nature. In addition to the various traditional methods used to harvest promising hydrogen fuel, the electrocatalytic hydrogen evolution reaction (HER) has been acknowledged as an environmentally friendly strategy because of its carbon emission-free nature, simple electrolysis process, and low operational potential.[4,5] Nevertheless, commercial implementation of HER has been limited by the exorbitant costs and limited availability of traditional noble electrode materials (Pt, Rh, Ir, and IrO_2).[6,7] Currently, there is substantial demand for alternative or metal-free electrodes with comparable and nondeteriorating electrochemical properties. Substantial research has been devoted to using earth-abundant nonmetal elements to reduce high overpotentials and manufacturing costs to meet social and economic needs.

In electrocatalytic HER, the electrolyte is one of the factors that determine water splitting performance since it provides the essential proton (H^+) as a result of reduction. It also offers a platform for charge transfer that generates hydrogen fuel efficiently via proton and electron binding. In general, acidic electrolyte (pH < 1) platforms are more favorable for HER due to their favorable kinetic rates.[8] However, a neutral medium (7 pH) is more desirable for grid-scale production, long-lasting device performance, and environmental safety. Unfortunately, the current water splitting approach relies heavily on valuable fresh water with acid or alkaline electrolytes for proton transfer.

Received: March 19, 2021
Revised: May 31, 2021

More importantly, it lacks environmental compatibility. Soaring water issues are an ongoing major and most serious water crisis, and using an acid electrolyte would be unrealistic for HER.[9]

Based on global energy requirements and the geographic availability of materials, the scientific community has focused its interest in seawater splitting.[10] Since it is a highly available natural electrolyte (salinity > 3.5%), seawater is thought to be the most suitable electrolyte candidate for large-scale hydrogen production.[9] Seawater contains 50% chloride, 48% sodium, and 2% of other elements such as magnesium and iron. However, performing HER is more challenging in seawater conditions because of the intrinsic low conductivity, ion poisoning, and high chloride corrosivity of seawater compared to the laboratory prototype (alkaline or acid electrolyte).[11] In particular, classic electrode materials fail to exhibit convincing long-term HER stability in seawater. Numerous reports have addressed electrolyte-assisted seawater splitting. Nevertheless, seawater splitting in the absence of an external electrolyte remains far from satisfactory, and only a few reports are available.[9,12−22] Therefore, the development of an electrode material that is inert and eternally robust under seawater conditions is of paramount importance. The electrode should (i) be highly HER-active in seawater, (ii) exhibit superior long-term saltwater stability, (iii) be able to withstand high current densities of 250 mA/cm^{2,} (iv) be stable and sustainable, and (v) be of low cost and abundant for compatibility with large-scale manufacturing and the ability to fulfill global energy harvesting demands.

Over the past few years, widespread research attention has been focused on transition metal dichalcogenides (TMDCs) because of their inherent water splitting properties inclusive of active sulfur sites, near-zero Gibbs free energy, excellent electrolyte stabilities, and thickness-dependent physical and chemical properties.[23,24] Among the various TMDCs, a two-dimensional (2D) layered VS_2 possesses an intrinsic metallic character and favors the effective transport of electrons. Further, basal and edge active sulfur sites of VS_2 enable the high specific active surface area.[3,25,26] Thus, VS_2 could be a promising electrocatalyst for water reduction applications than widely explored MoS_2.[27−29] Interestingly, the Gibbs free energy of the basal plane of VS^2 (ΔG_H = 0.16 eV) is fairly close to that of Pt (ΔG_H = 0.09 eV) and almost half of that of the basal plane of MoS_2 (ΔG_H = 0.189−1.92 eV).[28] The carbon-based skeleton is recognized as an ideal catalyst platform because of its excellent physical and chemical properties, as well as high electrochemical stability in all pH ranges.[30] Loading of a catalyst onto a stable carbon skeleton has produced numerous benefits, such as a large catalyst loading area, high electrocatalytic active surface area (ECSA), high electrochemical stability, and high conductivity for large-scale implementation of noble metal-free electrodes.[31]

Here, we report the fabrication of VS_2-decorated amorphous carbon (AC) via facile chemical vapor deposition for highly efficient, electrolyte-free direct seawater splitting. The well-tuned VS_2/AC heterostructure with ultrahigh edge active sites and superior electrical conductivity improves electrocatalytic water splitting performance. The VS_2/AC heterostructure serves as a superior electrocatalyst with an onset potential of 11 mV vs reversible hydrogen electrode (RHE). It produces 100 mA/cm^2 (η_{100}) at an overpotential of 71 mV vs RHE under 0.5 M $HClO_4$ acid electrolyte conditions. More significantly, VS_2/AC exhibits ultralong (50 h) stability during chronoamperometry (CA) studies. Furthermore, we evaluated the seawater splitting performance of the VS_2/AC heterostructure without an external electrolyte. The system delivered excellent HER performance with an onset potential of 56 mV vs RHE and η_{200} at an overpotential of 0.52 V vs RHE. Critically, we performed chronopotentiometry tests on the VS_2/AC heterostructure at an applied bias of 250 mA/cm^2 for 21 days under indoor and solar-powered outdoor conditions. Our device delivered superior stability and HER performance with negligible fluctuations. This indicates that TMDC/AC is a reliable electrode material for future electrocatalytic seawater splitting.

METHODS AND MATERIALS

AC was purchased from Sigma-Aldrich, and prior to chemical vapor deposition (CVD), the AC was cleaned via sequential (10 min each) ultrasonication in deionized water, acetone, isopropanol, and water. The VS_2 synthesis proceeded using a two-zone CVD furnace. VCl_3 (20 mg) and sulfur powder (80 mg) were used as precursors. The precursors were placed upstream (zone-I) and the AC was kept downstream (zone-II) of the gas flow (Figure S1) within the CVD reactor. VS_2 growth was performed for 15 min under an Ar/H_2 (10:1) carrier gas flow rate of 50 sccm. The temperature profile used is depicted in Figure S2. The temperature of zone-I (250 °C) reduced the VCl_3 and sulfur powder into V and sulfur vapors, which were transported toward the AC in zone-II (750 °C) by the uniform carrier gas flow. Random adatom adsorption onto the AC promoted subsequent VS_2 growth. Details of the growth mechanism are described elsewhere.[27]

Characterization Techniques. Surface morphology features were evaluated via field emission scanning electron microscopy (FESEM) using a Carl Zeiss ∑igma instrument and transmission electron microscopy (TEM) using an FEI-Tecnai G2F30 transmission electron microscope. Energy-dispersive X-ray spectroscopy (EDS) was performed using an Oxford Instruments Inca X-act. Raman spectra were recorded using a Renishaw InVia Raman spectrometer with a 532 nm excitation laser source. Chemical analysis was performed via X-ray photoelectron spectroscopy (XPS) using a Shimadzu ESCA 3400.

Device Fabrication and Electrochemical Analysis. Laboratory and real-time outdoor analyses were performed using three- and two-electrode systems, respectively. The synthesized VS_2/AC heterostructure, pristine AC, and saturated Ag/AgCl were employed as the working, counter, and reference electrodes, respectively. The three-electrode analyses were calibrated against the RHE using the equation $E_{RHE} = E_{Ag/AgCl} + E^0 + (0.059 \times pH)$ and iR corrected at 85%. All electrochemical characterizations were performed using a Biologic SP-150 potentiostat. Electrochemical impedance analysis was performed using a range of 0.1−10^4 Hz with an applied potential of −50 mV vs RHE. Chronoamperometry (CA) was performed at −50 mV vs RHE.

Gas Chromatography Analysis. Seawater electrocatalytic water splitting was performed in a custom-built, air-tight electrochemical cell. Gas chromatography (GC) analysis was performed using a Shimadzu GC 2014 with a thermal conductivity detector. Nitrogen was used as the reference gas at a continuous flow of 10 mL/min.

Computational Details. First-principles calculations were performed using the spin-polarized density functional theory as implemented in the Vienna ab-initio simulation package (projector-augmented wave method).[32,33] The exchange−correlation potential was treated using the Perdew−Burke−Ernzerhof generalized gradient approximation.[34] A plane-wave basis set with an energy cutoff of 550 eV and a 5 × 5 × 1 Monkhorst−Pack *k*-grid were used. Structural relaxation continued until the total energy and maximum atomic force converged to at least 10^{-4} eV per atom and 0.001 eV/Å, respectively. Henkleman's Bader charge analysis is used to study the charge in a given system.[35] A supercell approach with a 15 Å thick vacuum space along the *c*-axis was used to model the heterostructure.

https://doi.org/10.1021/acssuschemeng.1c01909
ACS Sustainable Chem. Eng. XXXX, XXX, XXX−XXX

Scheme 1. Schematic Representation of VS_2 Fabrication on AC by CVD

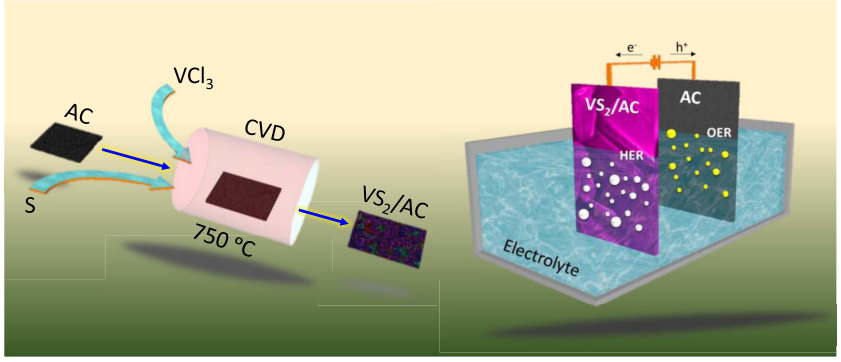

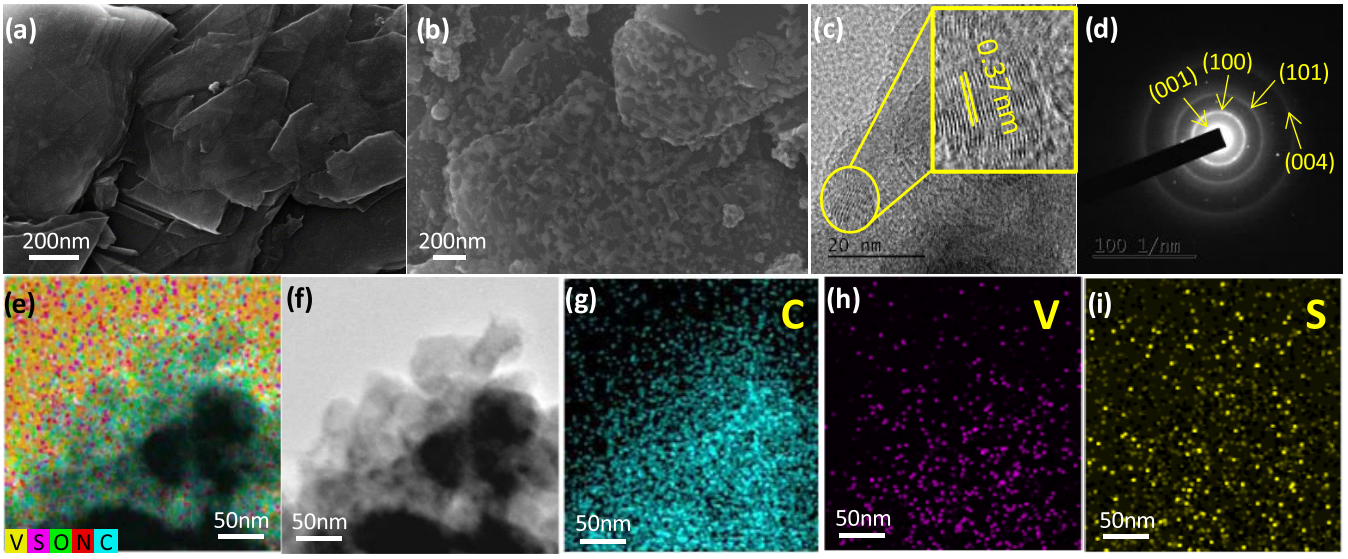

Figure 1. Morphological studies of VS_2/AC: FESEM images of (a) AC and (b) VS_2/AC, (c) HRTEM image of VS_2/AC, (d) SAED pattern of VS_2/AC, and (e–i) EDS elementary mapping of VS_2/AC.

RESULTS AND DISCUSSIONS

A schematic illustration of VS_2/AC synthesis is depicted in Scheme 1. Our goal is to grow highly uniform VS_2 on an AC substrate for seawater splitting. Uniform deposition and growth of VS_2 on AC are confirmed via FESEM (Figure 1a,b). The VS_2 particles with sizes ranging from 50 to 200 nm (Figure 1c) are observed as a result of coalescence and Oswald ripening of tiny VS_2 particles. HRTEM confirms the layered structure of VS_2 stacked on AC (Figure S3). This is evidenced by the bright and dark selected area electron diffraction (SAED) patterns seen in Figure 1d. The VS_2 *d*-spacing value is calculated to be 0.37 nm. This corresponds to the (001) crystallographic orientation of VS_2.[27] EDX was used to perform elemental analysis of VS_2/AC. Figures 1e–i and S4 show that V and S are distributed homogeneously on the carbon skeleton surface throughout the scanned region. In addition, the ratio of V and S is 1:1.9, which matches well with those of earlier reports.[28]

The Raman spectrum of bare AC is shown in Figure S5. It exhibits D-, G-, and 2D-band carbon fingerprint vibrations at 1350, 1576, and 2704 cm^{-1}, respectively.[36] The VS_2/AC heterostructure exhibits characteristic VS_2 at peaks 140, 281, and 405 cm^{-1}, which can be attributed to the E_{1g}, E_{2g}, and A_{1g} in-plane and out-of-plane VS_2 vibrations, respectively (Figure 2a).[17,37−40] Further, the X-ray diffraction (XRD) patterns of bare AC and VS_2/AC electrodes are shown in Figure 2b. Bare AC exhibits characteristic carbon peaks (2θ) at 26.5, 42.6, 44.7, and 54.7°, which are indexed to the (002), (100), (101), and (004) planes, respectively. The VS_2/AC heterostructure exhibits diffraction peaks at 17.9, 32, 37.2, and 41.4°, which correspond to (001), (100), (101), and (011) planes of VS_2, respectively, along with characteristic carbon diffraction peaks of AC.[17,38−40] The XRD pattern of VS_2/AC agrees well with JCPDS databases #47-1049 (AC) and #89-1640 (VS_2), and is consistent with the TEM analysis.

The C 1s peak is used as a reference for shift correction. The core-level binding energy spectra of C, S, and V are shown in Figure 2c–e. The *C* characteristic binding energy peaks that correspond to sp^2 and sp^3 hybridizations are located at 285.0 and 286.0 eV, respectively (Figure 2c). In addition, we observed C–O bonds at 288.3 eV that indicate surface oxidation. This can be corroborated by surface absorption of oxygen on AC (Figure 2c). Similarly, divalent prominent core-level orbital peaks of S $2p_{1/2}$ and S $2p_{3/2}$ are observed at 165.5 and 164.5 eV, respectively. In addition, the presence of two peaks at high binding energies of 166 and 169.3 eV can be attributed to the low-coordinate-state sulfur ions and metal sulfur, respectively (Figure 2d).[17,37,39−41] Further, strong V binding energy peaks at 517.4 and 522.0 eV belong to V $2p_{3/2}$ and V $2p_{1/2}$, respectively (Figure 2e).[42] The divalent peak

https://doi.org/10.1021/acssuschemeng.1c01909
ACS Sustainable Chem. Eng. XXXX, XXX, XXX−XXX

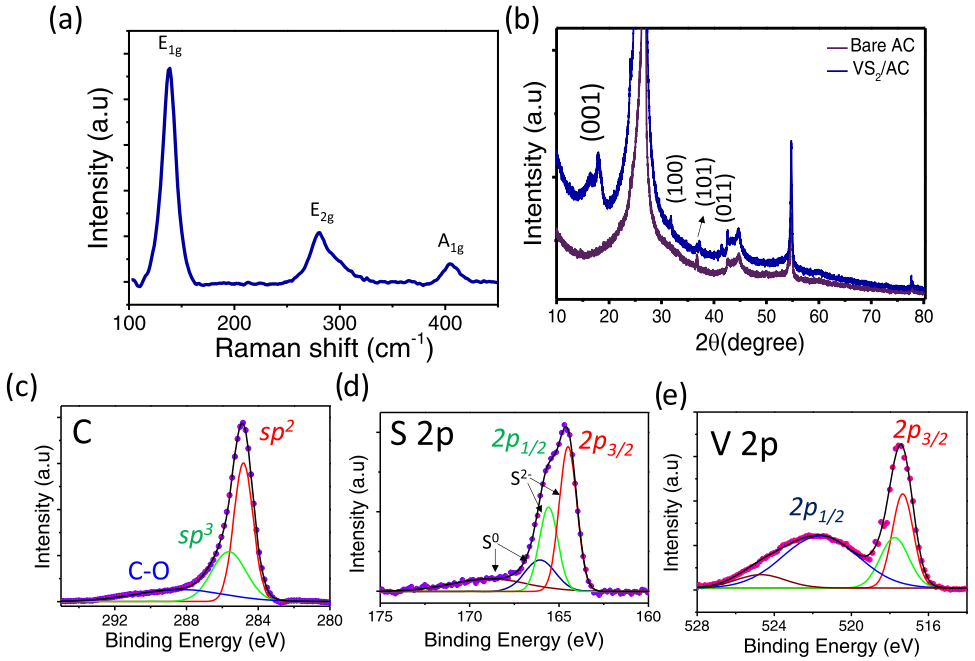

Figure 2. (a) Raman spectrum, (b) XRD pattern, and (c–e) region-specific XPS spectra of C, V, and S of VS_2/AC.

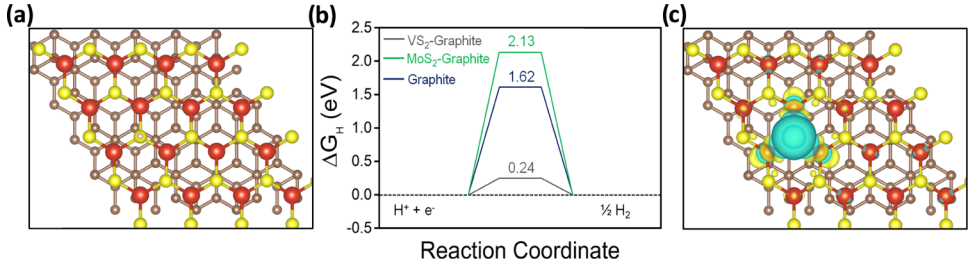

Figure 3. (a) VS_2/graphite heterostructure. Brown, red, yellow, and white spheres represent C, V, S, and H atoms, respectively. (b) ΔG_H for hydrogen adsorption on graphite, as well as the VS_2/graphite and MoS_2/graphite heterostructures. (c) Charge density differences for hydrogen adsorption on the VS_2/graphite heterostructure. Accumulation and depletion are denoted as yellow and blue isosurfaces (isovalue 4×10^{-3} e $Bohr^{-3}$).

corresponding to the core-level binding energy spectrum can be related to the V^{4+} and V^{2+} valency states.[41] The aforementioned characterization results confirm successful, broadly uniform CVD growth of 2D VS_2 on AC.

First-Principles Calculations. We employed first-principles calculations to understand hydrogen adsorption and to analyze the catalytic activity of a heterostructure consisting of a single layer of VS_2 on the top of a graphite stack (VS_2/graphite heterostructure). A good electrode material must possess a near-zero Gibbs free energy for easy release of hydrogen. The Gibbs free energy is defined as

$$\Delta G_H^* = E_{ads} + \Delta ZPE - T\Delta S_H \quad (1)$$

where E_{ads} is the adsorption energy of a hydrogen atom, ΔZPE is the change in the zero-point energy of hydrogen between the gas and the adsorbed states, and ΔS_H is the entropy of a hydrogen molecule in the gas phase. The value of $\Delta ZPE + (300\ K) \times \Delta S_H$ can be approximated as 0.24 eV.[43] Upon comparing various hydrogen adsorption sites on the VS_2 side of the VS_2/graphite heterostructure, we find that hydrogen prefers to adsorb on the top of sulfur sites (Figure 3a). The adsorption energy is given by

$$E_{ads} = E_{heterostructure+H} - E_{heterostructure} - 1/2\, E_H \quad (2)$$

where $E_{heterostructure+H}$ is the total energy of the relaxed heterostructure with the adsorbed hydrogen atom, $E_{heterostructure}$ is the total energy of the relaxed heterostructure, and E_H is the total energy of an isolated hydrogen molecule in the gas phase. The ΔG_H^* values obtained for graphite and the VS_2/graphite and MoS_2/graphite heterostructures are summarized in Figure 3b. In contrast to graphite (1.62 eV) and the MoS_2/graphite heterostructure (2.13 eV), the VS_2/graphite heterostructure achieves a small Gibbs free energy of 0.24 eV. The reason behind this small ΔG_H^* is the fast charge transfer between the VS_2/graphite heterostructure and the adsorbed hydrogen atom. From Bader charge analysis, sulfur atoms hold more charge in the VS_2/graphite (−0.68 e) than the MoS_2/graphite (−0.54 e) heterostructure. A charge density difference plot for the VS_2/graphite heterostructure is shown in Figure 3c.

HER Characterization. VS_2/AC HER examination was performed in fresh water using $HClO_4$ as the electrolyte (~0 pH). For comparison, the performances of MoS_2/AC, bare AC, and a commercial Pt rod were investigated using identical experimental parameters. As expected, VS_2/AC exhibits superior HER performance with a low onset potential of −11 mV vs RHE. This is distinctly lower than those of MoS_2/AC (−75 mV vs RHE) and pristine AC (−127 mV vs RHE) but slightly higher than that of commercial Pt (−7 mV vs

https://doi.org/10.1021/acssuschemeng.1c01909
ACS Sustainable Chem. Eng. XXXX, XXX, XXX−XXX

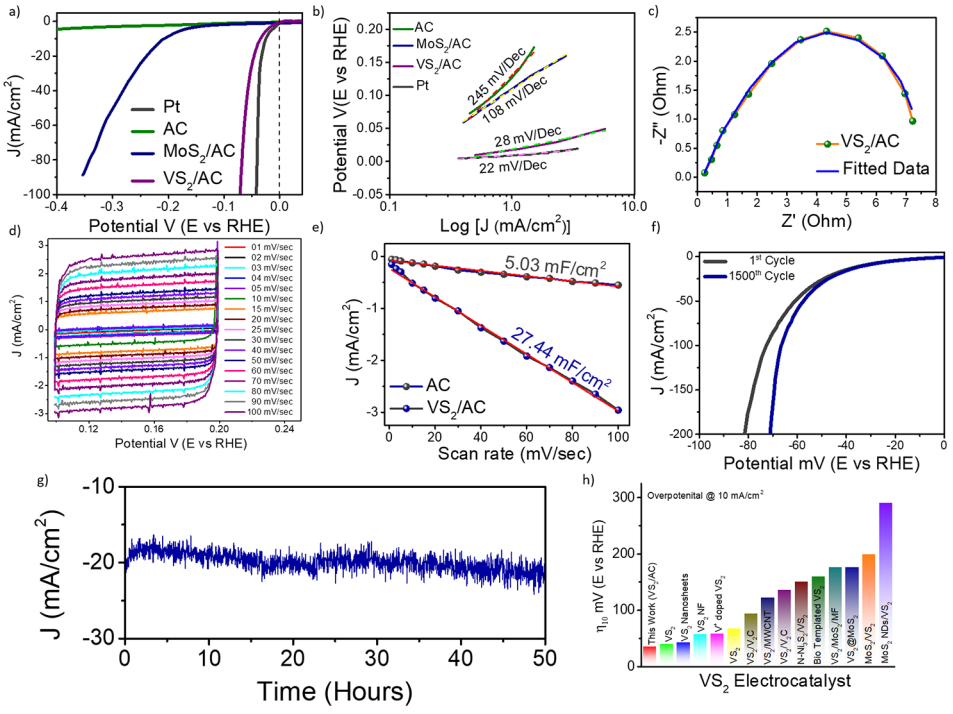

Figure 4. Electrocatalytic HER of VS_2/AC under 0.5 M $HClO_4$: (a) LSV, (b) LSV corresponding Tafel slope, (c) Nyquist plot recorded at the applied bias of −50 mV vs RHE, (d) CV recorded at various scan rates, (e) ECSA of VS_2/AC and bare AC, (f) LSV stability test comparison of the first cycle and the 1500th cycle, (g) CA of VS_2/AC recorded at a constant applied J of −50 mV vs RHE, and (h) comparative overpotential to attain −10 mA/cm^2 (η_{10}) of reported VS_2-based electrocatalysts.

RHE) (Figure 4a). The VS_2/AC electrocatalyst requires a small overpotential of −61 mV vs RHE to achieve a current density of −50 mA/cm^2 (η_{50}), while MoS_2/AC and pristine AC require −299 mV and −1.01 V vs RHE, respectively. In addition, both VS_2/AC and Pt exhibit small Tafel slope values of 28 and 22 mV/dec, respectively. It is thought that their kinetics follow the Volmer−Tafel rate-determination step for rapid hydrogen production. In comparison, bare AC and MoS_2/AC have been projected to follow the Volmer−Heyrovsky kinetic mechanism during hydrogen production, as they exhibit relatively large Tafel slopes of 105 and 245 mV/dec, respectively (Figure 4b).[7,44] The linear sweep voltammetry (LSV) and Tafel slope analysis directly evidence the superior HER performance of VS_2/AC caused by high-performing basal and edge active sulfur sites on the highly conductive carbon skeleton.[24,45]

Electrochemical impedance spectroscopy (EIS) was analyzed to study charge transfer. The Nyquist plot of VS_2/AC is depicted in Figure 4c. The equivalent circuit is drawn with electrical phase elements in Figure S7. R_S is the series resistance, while R_{CT} and C_{CT} are the charge transfer resistance and capacitance, respectively, at the electrolyte−material interface. The Nyquist plot and fitting indicate a low charge transfer resistance (R_{ct}) of 6.7 Ω for VS_2/AC. This is 12 and 70 times lower than that for MoS_2/AC and pristine AC, respectively (Figure S8). The small R_{ct} indicates that the availability of multiple active sulfur sites on VS_2/AC provides superior HER performance. In addition, the Nyquist plot confirms the monolithic nature of the heterostructure via the absence of interfacial resistance (R_S) at the AC−VS_2 junction.[5,46,47] Further, the ECSA is estimated from the double-layer capacitance (C_{dl}) at various scan rates in the non-Faradic region of 0.1−0.2 V vs RHE and depicted in Figures 4d and S9. It is well known that C_{dl} is proportional to the specific active area available to HER at the electrode/electrolyte interface.[26,48−52] The C_{dl} of VS_2/AC is estimated to be 27.44 mF/cm^2 (Figure 4e), which is seven times higher than that of standalone AC (5.03 mF/cm^2). This corroborates the availability of abundant VS_2/AC heterostructure active surface sites to sustained electrocatalytic hydrogen production.[53] Overall, inert ambient synthesis of 2D VS_2 using CVD produces an interfacial resistance-free junction along with strong coupling at the AC−VS_2 interface for significant HER performance and excellent charge transport toward the electrolyte, as revealed by LSV, EIS, and ECSA analyses.

Stability is an important electrocatalytic HER electrode material requirement. The long-term durability of VS_2 was evaluated over 1500 cycles. The results demonstrate superior LSV stability in acidic electrolyte conditions, with a negligible shift in the onset potential and a minor shift of −81 mV vs RHE at η_{200} (overpotential at 200 mA/cm^2) relative to the first cycle (Figure 4f). Furthermore, CA studies were carried out to analyze the stability of the VS_2/AC heterostructure at a constant potential of −50 mV vs RHE, as displayed in Figure 4g. The $J-T$ graph evidences the superior stability of the heterostructure for long-term applications. Further, the HER performance of the VS_2/AC heterostructure is compared to those of previously reported VS_2-based electrocatalysts in Table S1 and Figure 4h. The results highlight its outstanding performance, which is comparable to that of a Pt noble metal electrode. Overall, the electrocatalytic HER analysis of VS_2/AC in acidic electrolyte conditions evidences that the excellent hydrogen production ability of the heterostructure is comparable and consistent with commercial Pt, and thus VS_2/AC is appropriate for long-term device applications.

https://doi.org/10.1021/acssuschemeng.1c01909
ACS Sustainable Chem. Eng. XXXX, XXX, XXX−XXX

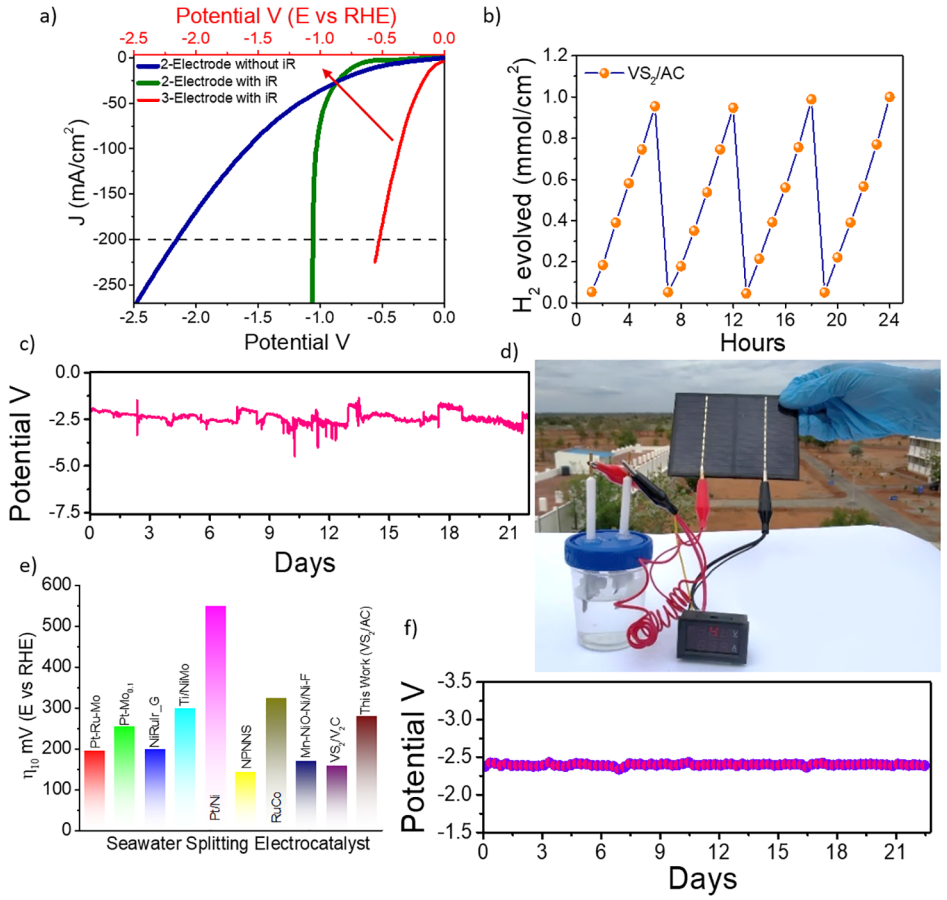

Figure 5. Natural seawater splitting of VS_2/AC: (a) comparative LSV results under two- and three-electrode systems, (b) GC analysis of VS_2/AC for the applied bias of −50 mA/cm^2, (c) CP at indoor conditions with an applied bias of −250 mA/cm^2 for a period of 21 days, (d) digital magnified image of outdoor seawater splitting, (e) comparison of overpotential at η_{10} of reported electrocatalyst materials, and (f) CP at outdoor conditions with an applied bias of −250 mA/cm^2 for a period of 21 days.

Natural Seawater Splitting. The oceans are the key to overcoming energy demand, as water electrolysis can be performed using a natural electrolyte. However, high efficiency is required for direct implementation in renewable energy applications. For HER analysis, seawater was collected from the shores of the Bay of Bengal in Nagapattinam, Tamil Nadu, India, and used without further purification or treatment. The pH of the collected seawater sample was 8.25, and its salinity was calculated to be 3.38%. The VS_2/AC electrocatalyst exhibits an onset potential of −56 mV vs RHE, and η_{200} (potential to reach −200 mA/cm^2) is achieved at −0.53 V vs RHE (Figure 5a). The Tafel slope is calculated to be 65 mV/dec (Figure S10) and is thought to follow the Volmer−Heyrovsky hydrogen production mechanism. EIS analysis indicates superior charge transfer and negligible resistance at the electrolyte−material junction (Figure S11). This corroborates the acidic electrolyte EIS analysis. We observe a high Tafel slope and R_{ct} gain under seawater conditions compared to the Tafel slope and R_{ct} noted under acidic electrolyte conditions. This can be ascribed to the high HER activation energy, poor conductivity, and low H^+ content of the natural electrolyte. To investigate the stability of the heterostructure under seawater conditions, we carried out 50 h of chronopotentiometry testing at a fixed current density of −100 mA/cm^2. The results reveal evidence of stable VS_2/AC HER performance under the natural electrolyte conditions (Figure S12).

A two-electrode configuration is more suitable for industrial-scale production owing to benefits such as straightforward operational procedures and cost-effectiveness. In this regard, we investigated two-electrode configuration LSV with VS_2/AC as the cathode and AC as the anode using seawater electrolyte (Figure 5a). In particular, VS_2/AC with iR (without iR) exhibits an onset potential of −0.26 (−0.11) V and achieves η_{250} at −1.06 (−2.1) V. Notably, LSV without iR produces a large-radius $J-V$ curve that can be attributed to uncompensated resistance at the electrode double layer.

Moreover, to ensure the absence of chlorine evolution and hypochlorite formation during the electrocatalytic reaction and to quantify hydrogen production, we performed GC analysis for 30 h using a constant applied bias of −50 mA/cm^2, and results are shown in Figure 5b. The absence of chlorine evolution and hypochlorite during seawater splitting was witnessed from the GC analysis with no obvious chlorine peak in the chromatogram (Figure S13). Most importantly, the ratio of O_2/H_2 of seawater splitting samples is in agreement with the standard calibration sample of a 1:2 ratio of O_2/H_2.[54] The hydrogen evolution rate of ∼0.97 mmol/cm^2 was observed for every 6 h of the reaction. It resulted in the Faradic efficiency (FE) of 62.7% under natural seawater electrolyte conditions. The corresponding FE calculations are

https://doi.org/10.1021/acssuschemeng.1c01909
ACS Sustainable Chem. Eng. XXXX, XXX, XXX−XXX

given in the Supporting Information. The low value of FE is attributed to the loss of charge transport, owing to pristine AC as the counter electrode. Our choice of AC as the counter electrode is to encourage an alternative to standard noble metal electrodes (Pt and Ir) since they are known to exhibit a high poisoning effect under seawater electrolyte conditions with poor reproducibility. Further, the possibilities of metal deposition on the working electrode from the Pt counter electrode are very high under given experimental conditions of applied potential.

To evaluate long-term large-scale HER production using VS_2/AC, we performed chronopotentiometry (CP) studies with an applied constant current of −250 mA/cm^2 in a two-electrode configuration for 21 days with a required potential of −2.5 ± 0.5 V (Figure 5c). Furthermore, we performed LSV periodically, confirming the inert nature of VS_2/AC during long-term seawater hydrogen production (Figure S14). However, we observe a thin layer of salt deposition on the VS_2/AC surface as a result of prolonged CP analysis (Figure S15). This blocks the active sulfur sites and increases the voltage required to reach η_{250} via an increase in the interfacial resistance. To maintain the working electrode, VS_2/AC was treated with 0.01 M HCl for 30 min once every 3 days. We also performed post-HER surface morphological characterization via FESEM and EDS mapping, and chemical composition by Raman spectroscopy for the VS_2/AC electrode, and the results are provided in Figures S16 and S17. FESEM images and the corresponding EDS mapping results confirm the presence of the VS_2 catalyst on the AC surface. Further, the post-HER Raman analysis of VS_2/AC is almost similar to that of an as-prepared sample and evidences superior VS_2/AC electrode stability even after long-term CP analysis and several acid treatments.

Further, to evaluate the real-time HER performance, solar-powered CP was evaluated at −250 mA/cm^2 for 3 weeks (7 A.M. to 6 P.M.), as illustrated in Figure 5d. The VS_2/AC electrocatalyst was powered by a commercial solar cell with a working range of 600 mA and 12 V. As expected, VS_2/AC exhibits excellent stability in CP studies when an overpotential of −2.4 ± 0.3 V (Figure 5f) is used to achieve a current density of 250 mA/cm^2. A real-time video clip of the measurement is shown in Supporting Movie M1. Comparisons to reported seawater electrocatalytic HER performances are given in Figure 5e and Table S2. The comparisons indicate that VS_2/AC exhibits excellent HER performance under electrolyte-free natural seawater conditions. It also exhibits stability superior to those reported for cathode materials in both indoor and solar-powered outdoor conditions.

It is worth noting that VS_2/AC offers abundant active sites on a conductive carbon skeleton. This heterostructure stimulates numerous benefits as it provides the active sites needed to overcome the kinetic barrier to HER under seawater conditions and delivers good stability owing to barrier-free interfacial charge transport between electrode and electrolyte. The flexible and hybrid electrode displays stability even after several hundred hours of device performance at high current densities and acid treatment to remove salt deposition.

CONCLUSIONS

In summary, highly entangled VS_2 deposited on an amorphous carbon skeleton via chemical vapor deposition was demonstrated to be an ideal electrode for electrocatalytic water splitting. The highly micrometric 3D matrix of AC with VS_2 is catalytically active in both acidic electrolyte and pristine seawater conditions. Our first-principles analysis evidenced that the VS_2/graphite heterostructure offers a near-zero Gibbs free energy and significant HER performance. LSV, ECSA, EIS, and stability analyses confirmed superior VS_2/AC heterostructure hydrogen production capabilities. It exhibited an outstanding HER performance during electrolyte-free seawater splitting with a high yield of ∼1 mmol/cm^2 for over 6 h and a maximum FE of 62.7%. Our analysis evidenced the inert nature of the catalyst in harsh electrolyte conditions, which is a critical requirement for long-term device applications. Due to its scalable synthesis, the VS_2/AC heterostructure can be a promising alternative to classical noble metal electrodes for large-scale and cost-effective seawater splitting.

ASSOCIATED CONTENT

Supporting Information

The Supporting Information is available free of charge at https://pubs.acs.org/doi/10.1021/acssuschemeng.1c01909.

Schematic representation of sample loading in a two-zone CVD furnace; growth temperature profile; VS_2/AC TEM images, FESEM EDS mapping, full-range Raman spectra; XPS survey spectra of VS_2/AC; equivalent circuit of VS_2/AC; Nyquist plot of MoS_2/AC and bare AC; ECSA of AC; Tafel slope and Nyquist plot of VS_2/AC under seawater conditions, 50 h of CP; GC spectra; Faradic efficiency calculation; periodic LSV; digital representation of salt deposition; post seawater splitting morphology and chemical composition analysis of and comparison tables (PDF)

Real-time video clip of the measurement (MP4)

AUTHOR INFORMATION

Corresponding Author

Jeganathan Kulandaivel − *Centre for Nanoscience and Nanotechnology, Department of Physics, Bharathidasan University, Tiruchirappalli 620024, Tamil Nadu, India;* orcid.org/0000-0003-4102-3439; Email: kjeganathan@yahoo.com, kjeganathan@bdu.ac.in

Authors

Paulraj Gnanasekar − *Centre for Nanoscience and Nanotechnology, Department of Physics, Bharathidasan University, Tiruchirappalli 620024, Tamil Nadu, India; Photonics Laboratory, Computer, Electrical and Mathematical Sciences and Engineering Division, King Abdullah University of Science and Technology (KAUST), Thuwal 23955-6900, Saudi Arabia;* orcid.org/0000-0001-5605-1542

Mathan Kumar Eswaran − *Physical Science and Engineering Division, King Abdullah University of Science and Technology (KAUST), Thuwal 23955-6900, Saudi Arabia*

Gayathri Palanichamy − *Centre for Nanoscience and Nanotechnology, Department of Physics, Bharathidasan University, Tiruchirappalli 620024, Tamil Nadu, India*

Tien Khee Ng − *Photonics Laboratory, Computer, Electrical and Mathematical Sciences and Engineering Division, King Abdullah University of Science and Technology (KAUST), Thuwal 23955-6900, Saudi Arabia;* orcid.org/0000-0002-1480-6975

https://doi.org/10.1021/acssuschemeng.1c01909
ACS Sustainable Chem. Eng. XXXX, XXX, XXX−XXX

Udo Schwingenschlögl − *Physical Science and Engineering Division, King Abdullah University of Science and Technology (KAUST), Thuwal 23955-6900, Saudi Arabia*

Boon S. Ooi − *Photonics Laboratory, Computer, Electrical and Mathematical Sciences and Engineering Division, King Abdullah University of Science and Technology (KAUST), Thuwal 23955-6900, Saudi Arabia*

Complete contact information is available at: https://pubs.acs.org/10.1021/acssuschemeng.1c01909

Notes

The authors declare no competing financial interest.

■ ACKNOWLEDGMENTS

K.J. thanks the FIST, PURSE, and Nanomission program of the Department of Science and Technology (DST), Ministry of Human Resource Development under Rashtriya Uchchatar Shiksha Abhiyan (RUSA 1.0), Alexander von Humboldt (AvH) Foundation, and DRDO for the financial support to develop the infrastructural facility. G.P. acknowledges DST-INSPIRE, Government of India, for the award of Senior Research Fellowship (DST INSPIRE-SRF IF#170198 DST/INSPIRE Fellowship/2016) and the KAUST Internship program BAS/1/1614-01-01.

■ REFERENCES

(1) Chen, Z.; Duan, X.; Wei, W.; Wang, S.; Ni, B. J. Recent Advances in Transition Metal-Based Electrocatalysts for Alkaline Hydrogen Evolution. *J. Mater. Chem. A* **2019**, *7*, 14971−15005.

(2) Liu, Y.; Wu, J.; Hackenberg, K. P.; Zhang, J.; Wang, Y. M.; Yang, Y.; Keyshar, K.; Gu, J.; Ogitsu, T.; Vajtai, R.; Lou, J.; Ajayan, P. M.; Wood, B. C.; Yakobson, B. I. Self-Optimizing, Highly Surface-Active Layered Metal Dichalcogenide Catalysts for Hydrogen Evolution. *Nat. Energy* **2017**, *2*, No. 17127.

(3) She, Z. W.; Kibsgaard, J.; Dickens, C. F.; Chorkendorff, I.; Nørskov, J. K.; Jaramillo, T. F. Combining Theory and Experiment in Electrocatalysis: Insights into Materials Design. *Science* **2017**, *355*, No. eaad4998.

(4) Anantharaj, S.; Ede, S. R.; Sakthikumar, K.; Karthick, K.; Mishra, S.; Kundu, S. Recent Trends and Perspectives in Electrochemical Water Splitting with an Emphasis on Sulfide, Selenide, and Phosphide Catalysts of Fe, Co, and Ni: A Review. *ACS Catal.* **2016**, *6*, 8069−8097.

(5) Gnanasekar, P.; Periyanagounder, D.; Kulandaivel, J. Vertically Aligned MoS 2 Nanosheets on Graphene for Highly Stable Electrocatalytic Hydrogen Evolution Reactions. *Nanoscale* **2019**, *11*, 2439−2446.

(6) Ramalingam, V.; Varadhan, P.; Fu, H. C.; Kim, H.; Zhang, D.; Chen, S.; Song, L.; Ma, D.; Wang, Y.; Alshareef, H. N.; He, J. H. Heteroatom-Mediated Interactions between Ruthenium Single Atoms and an MXene Support for Efficient Hydrogen Evolution. *Adv. Mater.* **2019**, *31*, No. 1903841.

(7) Varadhan, P.; Fu, H.; Priante, D.; Ramon, J.; Retamal, D.; Zhao, C.; Ebaid, M.; Ng, T. K.; Ajia, I.; Mitra, S.; Roqan, I. S.; Ooi, B. S.; He, J. H.; et al. Surface Passivation of GaN Nanowires for Enhanced Photoelectrochemical Water-Splitting. *Nano Lett.* **2017**, *17*, 1520−1528.

(8) You, B.; Sun, Y. Innovative Strategies for Electrocatalytic Water Splitting. *Acc. Chem. Res.* **2018**, *51*, 1571−1580.

(9) Guan, X.; Chowdhury, F. A.; Pant, N.; Guo, L.; Vayssieres, L.; Mi, Z. Efficient Unassisted Overall Photocatalytic Seawater Splitting on GaN-Based Nanowire Arrays. *J. Phys. Chem. C* **2018**, *122*, 13797−13802.

(10) Abdel-Aal, H. K.; Zohdy, K. M.; Kareem, M. A. Hydrogen Production Using Sea Water Electrolysis. *Open Fuel Cells J.* **2010**, *3*, 1−7.

(11) Kuang, Y.; Kenney, M. J.; Meng, Y.; Hung, W.-H.; Liu, Y.; Huang, J. E.; Prasanna, R.; Li, P.; Li, Y.; Wang, L.; Lin, M.; McGehee, M. D.; Sun, X.; Dai, H. Solar-Driven, Highly Sustained Splitting of Seawater into Hydrogen and Oxygen Fuels. *Proc. Natl. Acad. Sci. U.S.A.* **2019**, *116*, 6624−6629.

(12) Li, H.; Tang, Q.; He, B.; Yang, P. Robust Electrocatalysts from an Alloyed Pt-Ru-M (M = Cr, Fe, Co, Ni, Mo)-Decorated Ti Mesh for Hydrogen Evolution by Seawater Splitting. *J. Mater. Chem. A* **2016**, *4*, 6513−6520.

(13) Zheng, J.; Zhao, Y.; Xi, H.; Li, C. Seawater Splitting for Hydrogen Evolution by Robust Electrocatalysts from Secondary M (M = Cr, Fe, Co, Ni, Mo) Incorporated Pt. *RSC Adv.* **2018**, *8*, 9423−9429.

(14) Huang, Y.; Hu, L.; Liu, R.; Hu, Y.; Xiong, T.; Qiu, W.; Balogun, M. S.; Pan, A.; Tong, Y. Nitrogen Treatment Generates Tunable Nanohybridization of Ni5P4 Nanosheets with Nickel Hydr(Oxy)-Oxides for Efficient Hydrogen Production in Alkaline, Seawater and Acidic Media. *Appl. Catal., B* **2019**, *251*, 181−194.

(15) Niu, X.; Tang, Q.; He, B.; Yang, P. Robust and Stable Ruthenium Alloy Electrocatalysts for Hydrogen Evolution by Seawater Splitting. *Electrochim. Acta* **2016**, *208*, 180−187.

(16) Lu, X.; Pan, J.; Lovell, E.; Tan, T. H.; Ng, Y. H.; Amal, R. A Sea-Change: Manganese Doped Nickel/Nickel Oxide Electrocatalysts for Hydrogen Generation from Seawater. *Energy Environ. Sci.* **2018**, *11*, 1898−1910.

(17) Gao, S.; Li, G. D.; Liu, Y.; Chen, H.; Feng, L. L.; Wang, Y.; Yang, M.; Wang, D.; Wang, S.; Zou, X. Electrocatalytic H2 Production from Seawater over Co, N-Codoped Nanocarbons. *Nanoscale* **2015**, *7*, 2306−2316.

(18) Zhao, Y.; Jin, B.; Zheng, Y.; Jin, H.; Jiao, Y.; Qiao, S. Z. Charge State Manipulation of Cobalt Selenide Catalyst for Overall Seawater Electrolysis. *Adv. Energy Mater.* **2018**, *8*, No. 1801926.

(19) Yu, L.; Zhu, Q.; Song, S.; McElhenny, B.; Wang, D.; Wu, C.; Qin, Z.; Bao, J.; Yu, Y.; Chen, S.; Ren, Z. Non-Noble Metal-Nitride Based Electrocatalysts for High-Performance Alkaline Seawater Electrolysis. *Nat. Commun.* **2019**, *10*, No. 5106.

(20) Zheng, J. Pt-Free NiCo Electrocatalysts for Oxygen Evolution by Seawater Splitting. *Electrochim. Acta* **2017**, *247*, 381−391.

(21) Zhou, G.; Guo, Z.; Shan, Y.; Wu, S.; Zhang, J.; Yan, K.; Liu, L.; Chu, P. K.; Wu, X. High-Efficiency Hydrogen Evolution from Seawater Using Hetero-Structured T/Td Phase ReS2 Nanosheets with Cationic Vacancies. *Nano Energy* **2019**, *55*, 42−48.

(22) Hsu, S. H.; Miao, J.; Zhang, L.; Gao, J.; Wang, H.; Tao, H.; Hung, S. F.; Vasileff, A.; Qiao, S. Z.; Liu, B. An Earth-Abundant Catalyst-Based Seawater Photoelectrolysis System with 17.9% Solar-to-Hydrogen Efficiency. *Adv. Mater.* **2018**, *30*, No. 1707261.

(23) Chandrasekaran, S.; Yao, L.; Deng, L.; Bowen, C.; Zhang, Y.; Chen, S.; Lin, Z.; Peng, F.; Zhang, P. Recent Advances in Metal Sulfides: From Controlled Fabrication to Electrocatalytic, Photocatalytic and Photoelectrochemical Water Splitting and Beyond. *Chem. Soc. Rev.* **2019**, *48*, 4178−4280.

(24) Paulraj, G.; Venkatesh, P. S.; Dharmaraj, P.; Gopalakrishnan, S.; Jeganathan, K. Stable and Highly Efficient MoS2/Si NWs Hybrid Heterostructure for Photoelectrocatalytic Hydrogen Evolution Reaction. *Int. J. Hydrogen Energy* **2020**, *45*, 1793−1801.

(25) Pan, H. Metal Dichalcogenides Monolayers: Novel Catalysts for Electrochemical Hydrogen Production. *Sci. Rep.* **2014**, *4*, No. 5348.

(26) Liang, H.; Shi, H.; Zhang, D.; Ming, F.; Wang, R.; Zhuo, J.; Wang, Z. Solution Growth of Vertical VS2Nanoplate Arrays for Electrocatalytic Hydrogen Evolution. *Chem. Mater.* **2016**, *28*, 5587−5591.

(27) Ji, Q.; Li, C.; Wang, J.; Niu, J.; Gong, Y.; Zhang, Z.; Fang, Q.; Zhang, Y.; Shi, J.; Liao, L.; Wu, X.; Gu, O. L.; Liu, Z.; Zhang, Y. Metallic Vanadium Disulfide Nanosheets as a Platform Material for Multifunctional Electrode Applications. *Nano Lett.* **2017**, *17*, 4908−4916.

(28) Xu, J.; Zhu, Y.; Yu, B.; Fang, C.; Zhang, J. Metallic 1T-VS 2 Nanosheets Featuring V 2+ Self-Doping and Mesopores towards an

Efficient Hydrogen Evolution Reaction. *Inorg. Chem. Front.* **2019**, *6*, 3510−3517.
(29) Zhang, Y.; Chen, X.; Huang, Y.; Zhang, C.; Li, F.; Shu, H. The Role of Intrinsic Defects in Electrocatalytic Activity of Monolayer VS2 Basal Planes for the Hydrogen Evolution Reaction. *J. Phys. Chem. C* **2017**, *121*, 1530−1536.
(30) Kong, D.; Wang, H.; Lu, Z.; Cui, Y. CoSe 2 Nanoparticles Grown on Carbon Fiber Paper: An E Ffi Cient and Stable Electrocatalyst for Hydrogen Evolution Reaction. *J. Am. Chem. Soc.* **2014**, *136*, 4897−4900.
(31) Chei, B.; Li, X.; Li, X.; Yang, J.; Peng, W.; Dong, J.; Li, C.; Song, H. *RSC Adv.* **2016**, *6*, 60446−66053.
(32) Kresse, G.; Furthmüller, J. Efficiency of Ab-Initio Total Energy Calculations for Metals and Semiconductors Using a Plane-Wave Basis Set. *Comput. Mater. Sci.* **1996**, *6*, 15−50.
(33) Perdew, J. P.; Burke, K.; Ernzerhof, M. Generalized Gradient Approximation Made Simple. *Phys. Rev. Lett.* **1996**, *77*, 3865−3868.
(34) Blöchl, P. E. Projector Augmented-Wave Method. *Phys. Rev. B* **1994**, *50*, 17953−17979.
(35) Tang, W.; Sanville, E.; Henkelman, G. A Grid-Based Bader Analysis Algorithm without Lattice Bias. *J. Phys.: Condens. Matter* **2009**, *21*, No. 084204.
(36) Periyanagounder, D.; Gnanasekar, P.; Varadhan, P.; He, J. H.; Kulandaivel, J. High Performance, Self-Powered Photodetectors Based on a Graphene/Silicon Schottky Junction Diode. *J. Mater. Chem. C* **2018**, *6*, 9545−9551.
(37) Xu, J.; Yu, B.; Zhao, H.; Cao, S.; Song, L.; Xing, K.; Zhou, R.; Lu, X. Oxygen-Doped VS_4 Microspheres with Abundant Sulfur Vacancies as a Superior Electrocatalyst for the Hydrogen Evolution Reaction. *ACS Sustainable Chem. Eng.* **2020**, *8*, 15055−15064.
(38) Zhang, P.; Wang, L.; Wang, F.; Tan, D.; Wang, G.; et al. A Nonaqueous Na-Ion Hybrid Micro-Supercapacitor with Wide Potential Window and Ultrahigh Areal Energy Density. *Batteries Supercaps* **2019**, *2*, 918−923.
(39) Li, W.; Huang, J.; Feng, L.; Cao, L.; Liu, Y.; Pan, L. VS2 Nanoarchitectures Assembled by Single-Crystal Nanosheets for Enhanced Sodium Storage Properties. *Electrochim. Acta* **2018**, *286*, 131−138.
(40) Liao, J.-Y.; Manthiram, A. High-performance Na2Ti2O5 nanowire arrays coated with VS2 nanosheets for sodium-ion storage. *Nano Energy* **2015**, *18*, 20−27.
(41) Zhang, J.; Zhang, C.; Wang, Z.; Zhu, J.; Wen, Z.; Zhao, X.; Zhang, X.; Xu, J.; Lu, Z. Synergistic Interlayer and Defect Engineering in VS2 Nanosheets toward Efficient Electrocatalytic Hydrogen Evolution Reaction. *Small* **2018**, *14*, No. 1703098. 1-10.
(42) Masikhwa, T. M.; Barzegar, F.; Dangbegnon, J. K.; Bello, A.; Madito, M. J.; Momodu, D.; Manyala, N. Asymmetric Supercapacitor Based on VS2 Nanosheets and Activated Carbon Materials. *RSC Adv.* **2016**, *6*, 38990−39000.
(43) Bawari, S.; Kaley, N. M.; Pal, S.; Vineesh, T. V.; Ghosh, S.; Mondal, J.; Narayanan, T. N. On the Hydrogen Evolution Reaction Activity of Graphene-HBN van Der Waals Heterostructures. *Phys. Chem. Chem. Phys.* **2018**, *20*, 15007−15014.
(44) Shinagawa, T.; Garcia-Esparza, A. T.; Takanabe, K. Insight on Tafel Slopes from a Microkinetic Analysis of Aqueous Electrocatalysis for Energy Conversion. *Sci. Rep.* **2015**, *5*, No. 13801.
(45) Thomas, J. G. N. Kinetics of Electrolytic Hydrogen Evolution and the Adsorption of Hydrogen by Metals. *Trans. Faraday Soc.* **1961**, *57*, 1603.
(46) Guo, X.; Du, H.; Qu, F.; Li, J. Recent Progress in Electrocatalytic Nitrogen Reduction. *J. Mater. Chem. A* **2019**, *7*, 3531−3543.
(47) Gnanasekar, P.; Periyanagounder, D.; Varadhan, P.; He, J. H.; Kulandaivel, J. Highly Efficient and Stable Photoelectrochemical Hydrogen Evolution with 2D-NbS2/Si Nanowire Heterojunction. *ACS Appl. Mater. Interfaces* **2019**, *11*, 44179−44185.
(48) Anantharaj, S.; Ede, S. R.; Karthick, K.; Sam Sankar, S.; Sangeetha, K.; Karthik, P. E.; Kundu, S. Precision and Correctness in the Evaluation of Electrocatalytic Water Splitting: Revisiting Activity Parameters with a Critical Assessment. *Energy Environ. Sci.* **2018**, *11*, 744−771.
(49) Nandi, S.; Singh, S. K.; Mullangi, D.; Illathvalappil, R.; George, L.; Vinod, C. P.; Kurungot, S.; Vaidhyanathan, R. Low Band Gap Benzimidazole COF Supported Ni 3 N as Highly Active OER Catalyst. *Adv. Energy Mater.* **2016**, *6*, No. 1601189.
(50) Lukowski, M. A.; Daniel, A. S.; Meng, F.; Forticaux, A.; Li, L.; Jin, S. Enhanced Hydrogen Evolution Catalysis from Chemically Exfoliated Metallic MoS2 Nanosheets. *J. Am. Chem. Soc.* **2013**, *135*, 10274−10277.
(51) Lukowski, M. A.; Daniel, A. S.; English, C. R.; Meng, F.; Forticaux, A.; Hamers, R. J.; Jin, S. Highly Active Hydrogen Evolution Catalysis from Metallic WS2 Nanosheets. *Energy Environ. Sci.* **2014**, *7*, 2608−2613.
(52) Faber, M. S.; Dziedzic, R.; Lukowski, M. A.; Kaiser, N. S.; Ding, Q.; Jin, S. High-Performance Electrocatalysis Using Metallic Cobalt Pyrite (CoS 2) Micro- and Nanostructures. *J. Am. Chem. Soc.* **2014**, *136*, 10053−10061.
(53) Ahn, E.; Kim, B. Multidimensional Thin Film Hybrid Electrodes with MoS 2 Multilayer for Electrocatalytic Hydrogen Evolution Reaction. *ACS Appl. Mater. Interfaces* **2017**, *9*, 8688−8695.
(54) Wang, C.; Zhu, M.; Cao, Z.; Zhu, P.; Cao, Y.; Xu, X.; Xu, C.; Yin, Z. Heterogeneous Bimetallic Sulfides Based Seawater Electrolysis towards Stable Industrial-Level Large Current Density. *Appl. Catal., B* **2021**, *291*, No. 120071.

https://doi.org/10.1021/acssuschemeng.1c01909
ACS Sustainable Chem. Eng. XXXX, XXX, XXX−XXX